Australasian Physical & Engineering Sciences in Medicine (2019) 42:481–487
https://doi.org/10.1007/s13246-019-00744-7

SCIENTIFIC PAPER

A Monte Carlo study of pinhole collimated Cerenkov luminescence imaging integrated with radionuclide treatment

Changran Geng[1,2] · Yao Ai[1,2] · Xiaobin Tang[1,2] · Diyun Shu[1,2] · Chunhui Gong[1,2] · Fada Guan[3]

Received: 18 September 2018 / Accepted: 26 February 2019 / Published online: 4 March 2019

Abstract

Cerenkov luminescence imaging (CLI) is an emerging optical imaging technique, which has been widely investigated for biological imaging. In this study, we proposed to integrate the CLI technique with the radionuclide treatment as a "see-and-treat" approach, and evaluated the performance of the pinhole collimator-based CLI technique. The detection of Cerenkov luminescence during radionuclide therapy was simulated using the Monte Carlo technique for breast cancer treatment as an example. Our results show that with the pinhole collimator-based configuration, the location, size and shape of the tumors can be clearly visualized on the Cerenkov luminescence images of the breast phantom. In addition, the CLI of multiple tumors can reflect the relative density of radioactivity among tumors, indicating that the intensity of Cerenkov luminescence is independent of the size and shape of a tumor. The current study has demonstrated the high-quality performance of the pinhole collimator-based CLI in breast tumor imaging for the "see-and-treat" multi-modality treatment.

Keywords Cerenkov luminescence imaging · Monte Carlo · Breast tumor · Radionuclide therapy

Introduction

Cerenkov luminescence occurs when a charged particle travels through a medium with a velocity greater than the group speed of light in the medium [1]. Charged particles can be produced either from the decay of radionuclides directly or from secondary charged particles of high energy radiations in medical application. With the improved sensitivity of the optical detectors [e.g., highly sensitive charge-coupled device (CCD) and electron-multiplying charge-coupled device (EMCCD)], Cerenkov luminescence imaging (CLI) has been exploited as an optical imaging modality for small animals [2–6] and also in the biomedical field of human studies [7, 8]. CLI is based on the detection of Cerenkov luminescence, which is usually generated by radiations from radiopharmaceuticals labeled with beta radioisotopes [2, 8–10]. CLI has been mostly applied in preclinical studies, e.g., the tumor localization [9] and the radionuclide uptake monitoring in small living animals [11]. For human studies, Cerenkov luminescence can be used for endoscopic imaging [12], external imaging of ^{131}I in the thyroid, [13] and image guided tumor resection surgery [14]. As a functional imaging modality, the CLI also has some advantages such as its low-cost and easy-to-operate characteristics compared with other imaging modalities such as the positron emission tomography (PET) and single photon emission computed tomography (SPECT) [15]. For a typical beta-emitting radionuclide (e.g., ^{90}Y and ^{131}I), approximately 1–100 optical photons can be produced per decay [16].

The emergence of radionuclide-labeled nanomedicines has been rapidly increasing over the past decades because their application in cancer diagnosis and treatment has the great potential to improve cancer outcomes. It is desired to image the distribution of targeted radiotherapeutic agents in a patient's body prior to or during the treatment for optimizing the treatment strategies and determining the suitability of a given agent for a particular patient. Although pre-targeting

Changran Geng and Yao Ai contributed equally to this work.

✉ Xiaobin Tang
tangxiaobin@nuaa.edu.cn

[1] Department of Nuclear Science and Engineering, Nanjing University of Aeronautics and Astronautics, Nanjing 210016, China

[2] Collaborative Innovation Center of Radiation Medicine of Jiangsu Higher Education Institutions, Nanjing 210016, China

[3] Department of Radiation Physics, The University of Texas MD Anderson Cancer Center, Houston, TX 77030, USA

and imaging prior to the treatment is the common way to design the treatment strategy, integrating a "see-and-treat" modality can improve the treatment efficiency and reduce the potential side effects caused by the pre-imaging process. Considering the "free" information of Cerenkov photons from the radioisotopes, CLI has the potential to become a useful tool for the multi-modality treatment using a single radiolabeled molecule. In this work, we have assessed the potential of the pinhole collimator-based CLI technique for the tumor imaging during radionuclide therapy for the novel "see-and-treat" treatment modality for breast cancer.

Materials and methods

Monte Carlo simulation

The Geant4 Monte Carlo (MC) toolkit (version 4.10.4.p02) [17, 18] was used to simulate the particle transport and CLI of breast tumors. Geant4 is a general-purpose Monte Carlo simulation toolkit for particle transport and it has been widely used in the field of medical physics. In the current study, the "standard low-energy electromagnetic physics" and "optical physics" processes (G4Cherenkov and G4OpAbsorption classes) were applied to simulate the transport of both ionizing radiations and optical photons. The wavelength of Cherenkov photons in the simulations ranges from 450 to 650 nm. The production threshold of secondary particles was set as 0.01 mm. The radionuclide ^{90}Y (β^- emitter) emitting 2.2 MeV end-point energy was selected as the input particle source, and the number of radionuclide decays was set to 1×10^9 for each simulation run [19]. The simulation time was approximately 12 h for each simulation run using a 64-thread workstation.

Breast voxel phantom

To simulate a breast cancer patient, a radiation reference human phantom with breast tumor(s) was established based on the 30-year-old CHRP-female phantom [20, 21] (Fig. 1). The voxel size is $0.2\times0.2\times0.2$ mm^3 in this mesh phantom. The elemental compositions of tissues and organs were obtained from the references of ICRU-46 and ICRP-89 [22, 23]. Tumors were assumed to be located in the upper-lateral quadrant of the right breast (Fig. 1). The ^{90}Y source was uniformly distributed within the region of malignant tissue for simulating the ^{90}Y-DOTATOC treatment. Optical properties (i.e., the absorption coefficient and the scattering coefficient) were applied to each segmented volume. Optical properties of normal and malignant human breast tissues were based on measured values from the study by Ghosh et al. [24], and optical properties of the soft tissue, skin, and muscle were found from the study by Bashkatov et al. [25, 26] (Fig. 2).

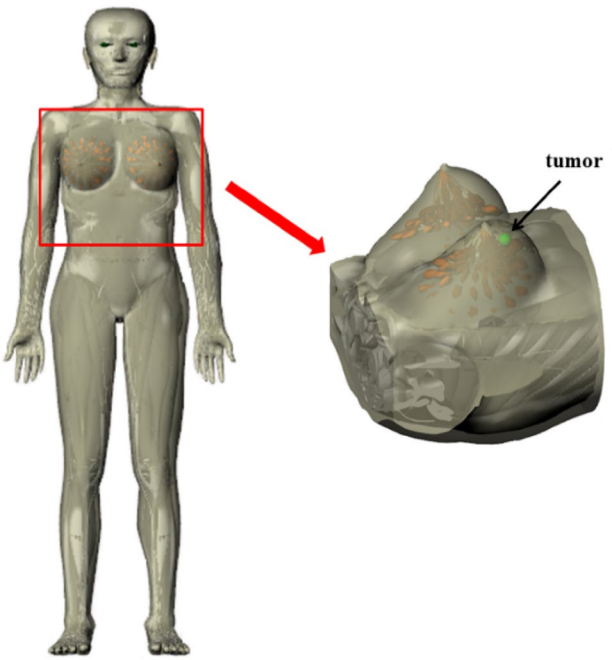

Fig. 1 The 30-year-old CHRP-female phantom with a tumor located in the upper-lateral quadrant of the right breast

A constant refractive index of $n=1.4$, which is the average value in all human tissues, was applied to all of the voxels in the phantom [14, 27]. The anisotropy factor g was set to 0.9 in accordance with the study by Sandell et al. [28].

Cerenkov luminescence imaging settings

A pinhole collimator-based camera was selected to capture Cerenkov luminescence generated from radionuclides in breast tumors [27], as shown in Fig. 3. The diameter of the pinhole is 1 mm. The distance between the phantom and the hole is 6 cm, and the distance from the detector to the hole is 6 cm. The size of the detector array is 10.24 cm × 10.24 cm, which has a pixel size of 0.1 mm × 0.1 mm.

Results

CLI performance for localized tumor cases at various depths

The CLIs of a single tumor site located at the depth of 1, 2.5, 5, and 7.5 mm are shown from Fig. 4a–d, respectively. The signal of Cerenkov light intensity decreases with the increase of the depth of tumor. This is due to the attenuation of Cerenkov photons in tissue. The detection efficiency of Cerenkov photons as a function of the tumor depth in the breast are shown in Fig. 5. The linearity in this semi-log

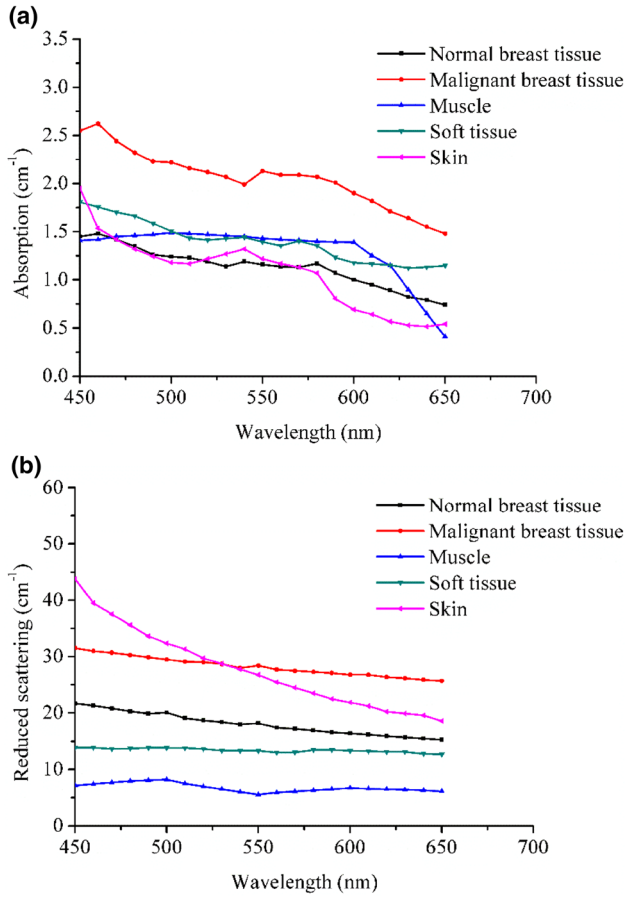

Fig. 2 The absorption coefficient and reduced scattering coefficient of different types of tissue

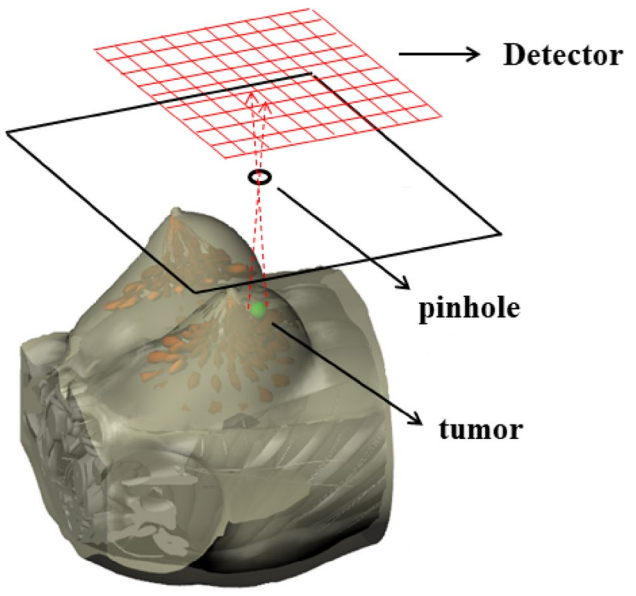

Fig. 3 Schematic of the Cerenkov luminescence imaging using a pinhole collimator-based camera with a detector array

plot reveals that the signal decreases exponentially with the tumor depth.

CLI performance for metastatic tumor cases with various concentrations of radionuclides

To explore the CLI quality for metastasis (i.e., multiple tumors), two solid tumors with the same size were assumed under the same depth. Figure 6a, b show the CLI of multiple tumors and the Cerenkov luminescence intensity profiles at the center of the image assuming the same radioactivity within these two tumors. Figure 6c, d illustrate the CLI of multiple tumors and the Cerenkov luminescence intensity profile at the center of the image when the ratio of radioactivities of two tumors is 2:1, respectively. It can be found that the ratio of peak value of Cerenkov luminescence intensity profile is the same as the density of radioactivity set in tumors from Fig. 6a–d, when the radioactivity ratio is set as 1:1 and 2:1, respectively. Furthermore, when the radioactivity ratio of 3:1 and 4:1 is investigated, the results also show the consistency between the Cerenkov luminescence intensity and the density of radioactivity in tumors.

CLI of multiple tumors at different depths and shapes

To explore the CLI quality of multiple tumors, a case with two tumors located at different depths (0.5 cm and 2 cm below the skin) was established. Figure 7a, b show the CLIs of multiple tumors and the Cerenkov luminescence intensity profile at the center of the image in the case of different distances respectively. The profile peak value decreases with the increased tumor depth for the metastatic tumor. This observation is caused by the increased attenuation of optical photons for a deeper tumor. To account for the attenuation effect, a possible method is to perform the image reconstruction with multiple images from different detection directions with different attenuation depths. To simulate the effect of CLI on the irregularity of the tumor, two tumors with the shape of sphere and ellipsoid were embedded in breast respectively. Figure 8 shows the CLI of the tumors with the shape of sphere and ellipsoid. The image shows clear profiles of tumors.

Discussion

Using radionuclide labeled Nano-medicine to treat cancer is an emerging type of targeted radiation therapy modality which has shown promising outcome in recent years [8, 11]. In order to make a cancer drug that can be administered as planned for a better balance of the treatment efficacy and the side-effects, it is desirable to inquire the internal

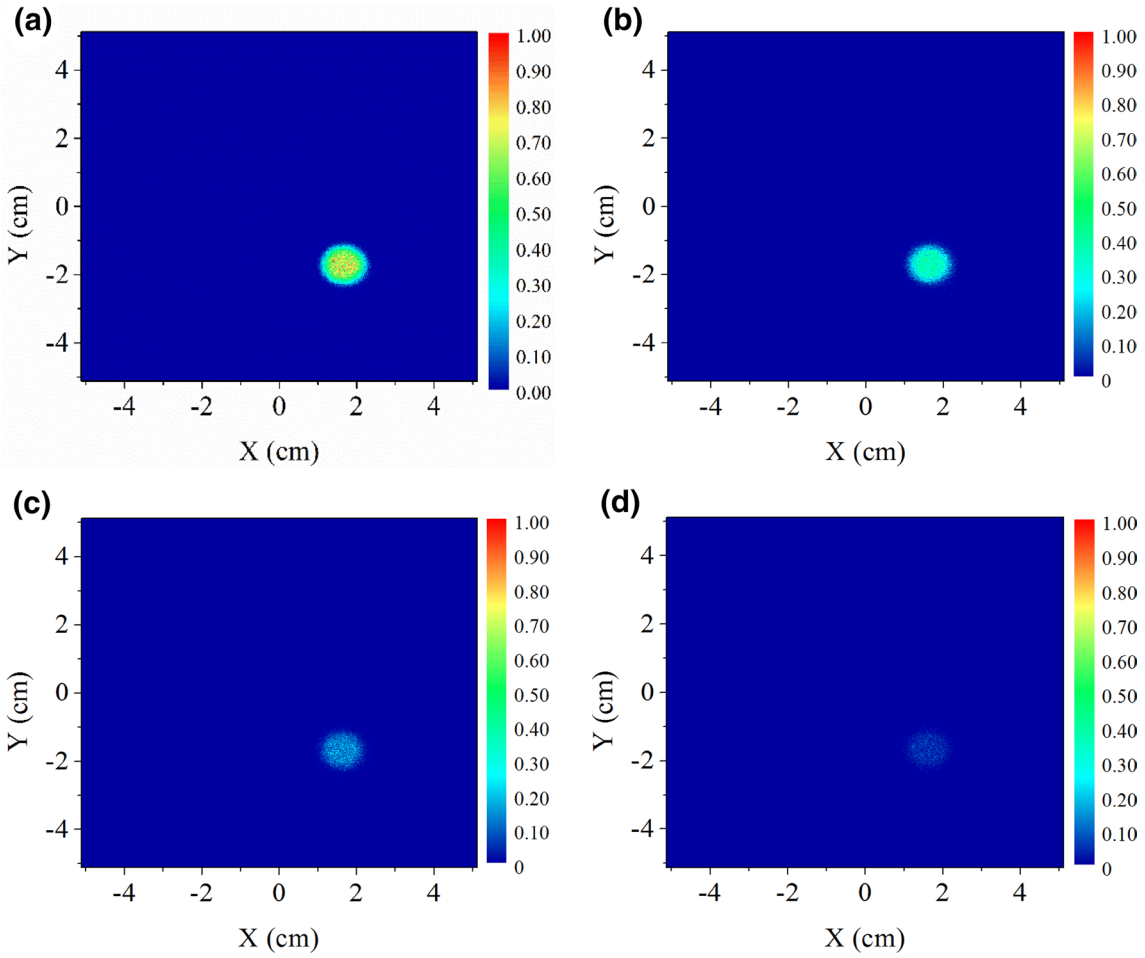

Fig. 4 The CLI of tumors at the depth of 1 mm, 2.5 mm, 5 mm, and 7.5 mm

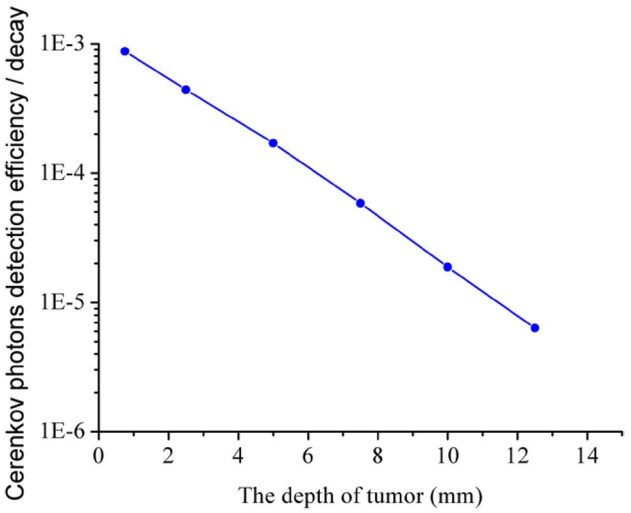

Fig. 5 The detection efficiency of Cerenkov photons as a function of tumor depth

distribution of the targeted agents in both animal studies and patient treatment. Cherenkov luminescence imaging has already been a useful tracing probe tool for animal studies. The light yield of the beta-emitters of radionuclide is tens to hundreds of optical photons per decay over the wide range of wavelength of Cerenkov radiation [16]. With different tissue types and different energies of the beta particle, the amount of Cerenkov light can be quite different. For clinical radionuclide therapy, when beta-emitter based nuclide medicine was used, the CLI technique can also be applied along with prior to the treatment or during the treatment, to conduct the "see-and-treat" radiotherapy. There are twofold meanings for the "see-and-treat" technique. The first one is that the CLI can be obtained before the treatment with a relatively low dose, and the distribution of the medicine can be known with the obtained CLI, which will be useful for further prediction of the treatment outcome. The second one is that the CLI can be conducted during the treatment for real-time dose reconstruction, which is similar to the work published by Balkin et al. [29].

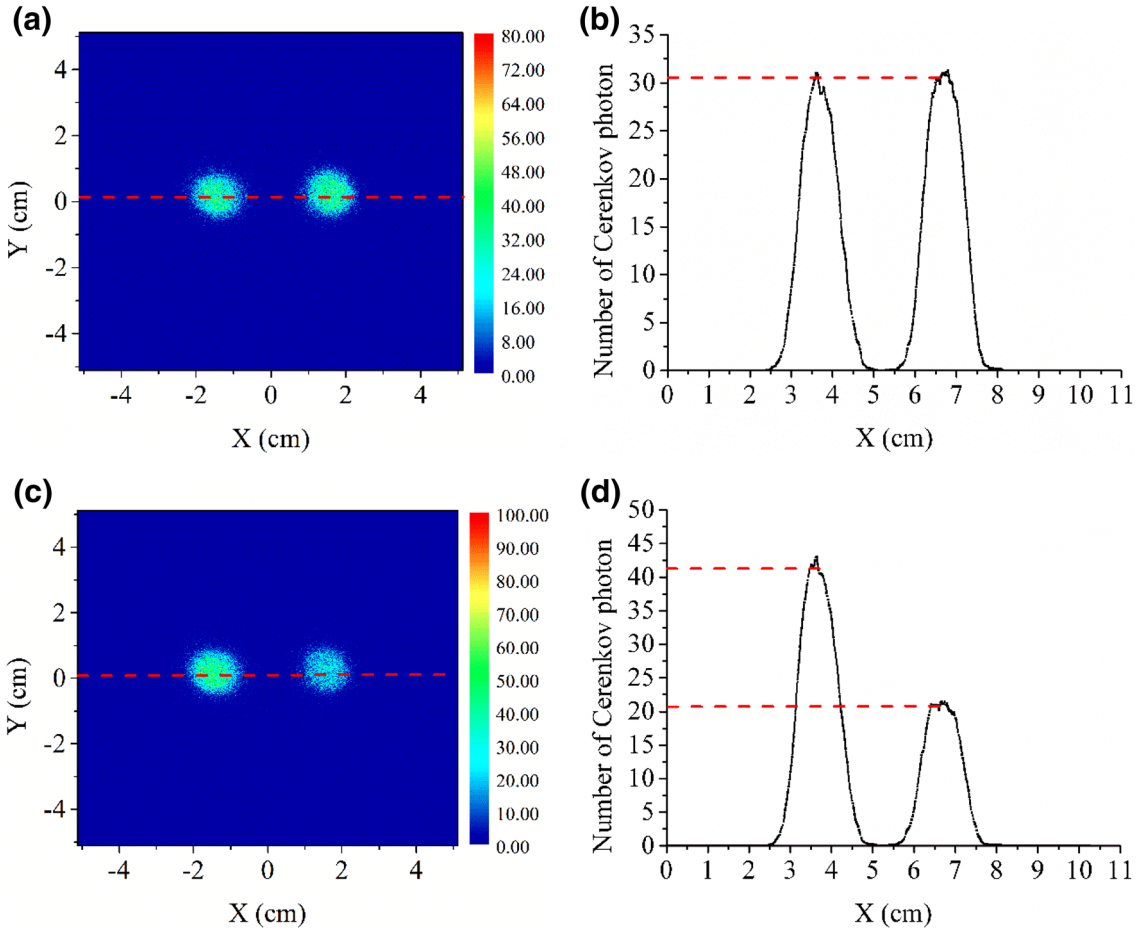

Fig. 6 The CLI for the case of radioactivity ratio is 1:1 between two tumors (**a**), and the Cerenkov luminescence intensity profile of the CLI (**b**). The CLI for the case of radioactivity ratio is 2:1 between two tumors (**c**), and the Cerenkov luminescence intensity profile of the CLI (**d**)

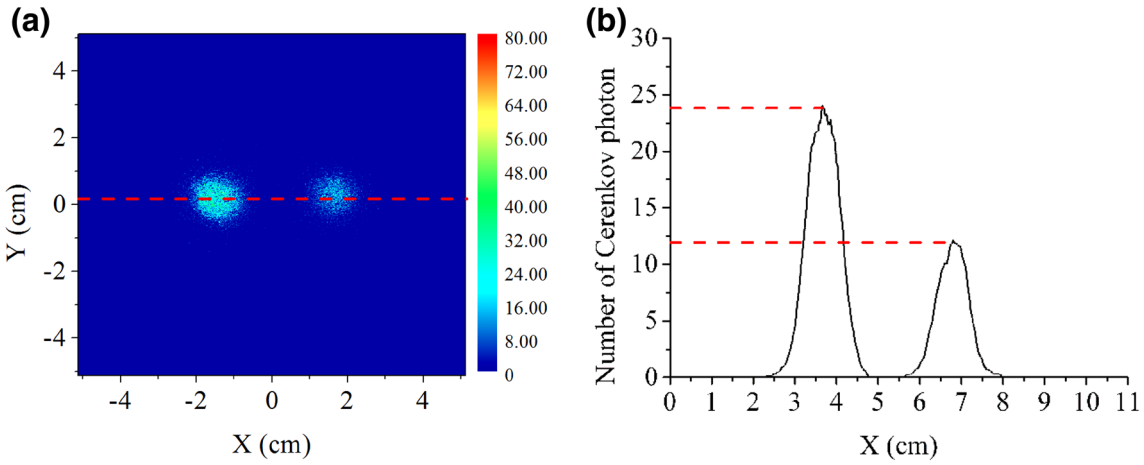

Fig. 7 The CLI of tumors located at the depth of 0.5 cm and 2 cm (**a**), and the Cerenkov luminescence intensity profile of the CLI (**b**)

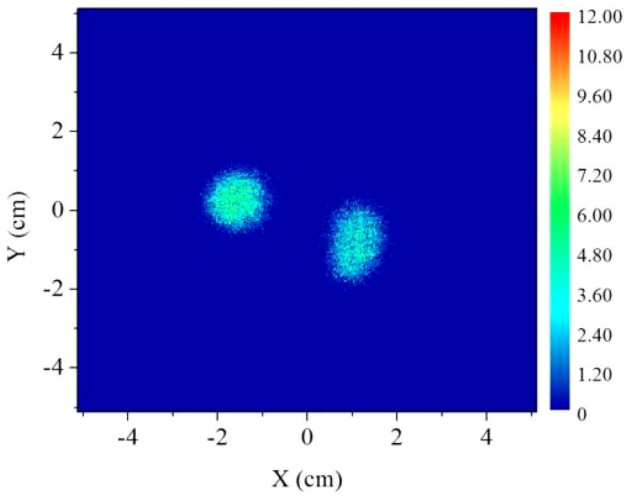

Fig. 8 The CLI of the tumors with the shape of sphere and ellipsoid

In this study, we took the breast cancer as an illustrative example to explore the feasibility of using the CLI to implement the "see-and-treat" technique. We used a pinhole collimator-based photon detector configuration to simulate the CCD configuration and also the pinhole collimator system. Using a pinhole camera for imaging the Cerenkov photons is advantageous on the infinite depth of field, and also there is no vignetting effect. The spatial resolution will be determined by the size of the hole. Nevertheless, the efficiency is lower than using the lens-based CCD camera, which needs to be further investigated through experiments.

From the results we can find that with tumors localized in different depth, the signal of Cerenkov radiation detected by the external camera decreases exponentially. For tumors of different sizes, the signal detected by the camera shows a linear relationship for the same depth location. As demonstrated from the Figs. 6, 7, 8, the Cerenkov radiation can clearly show the contour (shape) of the tumor, which indicates the potential application of visualizing the distribution of the radionuclide with the drug delivered. For the conditions of multiple tumors at different depths, the detected signal shows difference for the two tumors. Considering the attenuation of optical photons, using data from multiple directions can reconstruct the distribution and will be beneficial for volumetric visualization. Even that the imaging technique in this study was obtained as a two-dimensional image, there are some studies with the technique to show the depth information about the source from CLI [30], which will be investigated in future studies. The noise and background distribution, which might affect the results, were not included in the study.

It should be noted that one of the limitations of applying CLI is the weak penetrations of the Cerenkov luminescence in biological tissues (a few millimeters only). Therefore, the CLI is likely to be more suitable for the shallower tumors (e.g., the case presented in the current work). Detailed experimental studies should be performed, and various practical issues need to be explored in future studies prior to the clinical application of CLI.

Conclusions

Radionuclide therapy has been a promising cancer treatment modality with the the emergence of Nano-medicine and other novel techniques. To study the feasibility of the multi-modality treatment, which may potentially provide the "see-and-treat" with a single molecule using CLI, we have explored the performance of the pinhole collimator-based CLI for the case of breast tumors during the radionuclide therapy. Our results indicate that the images of Cerenkov luminescence could be used to visualize the location, size and shape of tumors for the explored situations. The detection efficiency of Cerenkov photons decreases with the increase of the depth of tumor in tissues. The current study has demonstrated the feasibility of the pinhole collimator-based CLI in breast tumor imaging for the "see-and-treat" multi-modality treatment.

Funding This work was supported by the National Natural Science Foundation of China (Grant No. 11805100), and the National Key Research and Development Program (Grant No. 2016YFE0103600 and No. 2017YFC0107700).

Compliance with ethical standards

Conflict of interest The authors declare that they have no conflicts of interest.

Ethical approval This article does not contain any studies with human participants and animals performed by any of the authors.

References

1. Cherenkov PA (1934) Visible emission of clean liquids by action of γ radiation. Dokl Akad Nauk SSSR 2:451
2. Spinelli AE, D'Ambrosio D, Calderan L et al (2010) Cerenkov radiation allows in vivo optical imaging of positron emitting radiotracers. Phys Med Biol 55(2):483–495. https://doi.org/10.1088/0031-9155/55/2/010
3. Boschi F, Spinelli AE, D'Ambrosio D et al (2009) Combined optical and single photon emission imaging: preliminary results. Phys Med Biol 54(23):L57–L62. https://doi.org/10.1088/0031-9155/54/23/L01
4. Spinelli AE, Lo Meo S, Calandrino R et al (2011) Optical imaging of Tc-99m-based tracers: in vitro and in vivo results. J Biomed Opt 16(11):116023. https://doi.org/10.1117/1.3653963

5. Holland JP, Normand G, Ruggiero A et al (2011) Intraoperative imaging of positron emission tomographic radiotracers using Cerenkov luminescence emissions. Mol Imaging 10(3):177–186
6. Cao X, Li Y, Zhan YH et al (2016) Removing noises induced by gamma radiation in cerenkov luminescence imaging using a temporal median filter. Biomed Res Int. https://doi.org/10.1155/2016/7948432
7. Liu HG, Ren G, Miao Z et al (2010) Molecular optical imaging with radioactive probes. Plos ONE 5 (3):e9470
8. Boschi F, Calderan L, D'Ambrosio D et al (2011) In vivo F-18-FDG tumour uptake measurements in small animals using Cerenkov radiation. Eur J Nucl Med Mol Imaging 38(1):120–127
9. Robertson R, Germanos MS, Li C et al (2009) Optical imaging of Cerenkov light generation from positron-emitting radiotracers. Phys Med Biol 54(16):N355–N365
10. Spinelli AE, Boschi F, D'Ambrosio D et al (2011) Cherenkov radiation imaging of beta emitters: in vitro and in vivo results. Nucl Instrum Methods A 648:S310–S312
11. Hu ZH, Ma XW, Qu XC et al (2012) Three-dimensional noninvasive monitoring iodine-131 uptake in the thyroid using a modified Cerenkov luminescence tomography approach. Plos ONE 7(5):e37623
12. Liu HG, Carpenter CM, Jiang H et al (2012) Intraoperative imaging of tumors using Cerenkov luminescence endoscopy: a feasibility experimental study. J Nucl Med 53(10):1579–1584
13. Spinelli AE, Ferdeghini M, Cavedon C et al (2013) First human Cerenkography. J Biomed Opt 18(2):020502.
14. Klein JS, Mitchell GS, Cherry SR (2017) Quantitative assessment of Cerenkov luminescence for radioguided brain tumor resection surgery. Phys Med Biol 62(10):4183–4201. https://doi.org/10.1088/1361-6560/aa6641
15. Hu Z, Liang J, Yang W et al (2010) Experimental Cerenkov luminescence tomography of the mouse model with SPECT imaging validation. Opt Express 18(24):24441–24450. https://doi.org/10.1364/OE.18.024441
16. Gill RK, Mitchell GS, Cherry SR (2015) Computed Cerenkov luminescence yields for radionuclides used in biology and medicine. Phys Med Biol 60(11):4263–4280
17. Allison J, Amako K, Apostolakis J et al (2006) Geant4 developments and applications. IEEE Trans Nucl Sci 53(1):270–278
18. Agostinelli S, Allison J, Amako K et al (2003) GEANT4-a simulation toolkit. Nucl Instrum Methods A 506(3):250–303
19. Ai Y, Tang X, Shu D et al (2017) Measurement of dose in radionuclide therapy by using Cerenkov radiation. Australas Phys Eng Sci Med 40(3):695–705. https://doi.org/10.1007/s13246-017-0579-6
20. Geng CR, Tang XB, Hou XX et al (2014) Development of Chinese hybrid radiation adult phantoms and their application to external dosimetry. Sci China Technol Sci 57(4):713–719
21. Guitton TG, Kinaci A, Ring D (2013) Diagnostic accuracy of 2- and 3-dimensional computed tomography and solid modeling of coronoid fractures. J Shoulder Elbow Surg 22(6):782–786
22. Bethesda MD (1992) Photon, electron, proton and neutron interaction data for body tissues. ICRU 46
23. Valentin J (2002) Basic anatomical and physiological data for use in radiological protection: reference values: ICRP Publication 89. Ann ICRP 32:1–277
24. Ghosh N, Mohanty SK, Majumder SK et al (2001) Measurement of optical transport properties of normal and malignant human breast tissue. Appl Opt 40(1):176–184
25. Bashkatov AN, Genina EA, Kochubey VI et al (2005) Optical properties of human skin, subcutaneous and mucous tissues in the wavelength range from 400 to 2000 nm. J Phys D Appl Phys 38(15):2543–2555
26. Bashkatov AN, Genina EA, Tuchin VV (2011) Optical properties of skin, subcutaneous, and muscle tissues: a review. J Innov Opt Health Sci 4(1):9–38
27. Helo Y, Rosenberg I, D'Souza D et al (2014) Imaging Cerenkov emission as a quality assurance tool in electron radiotherapy. Phys Med Biol 59(8):1963–1978
28. Sandell JL, Zhu TC (2011) A review of in-vivo optical properties of human tissues and its impact on PDT. J Biophotonics 4(11–12):773–787
29. Balkin ER, Kenoyer A, Orozco JJ et al (2014) In vivo localization of Y-90 and Lu-177 radioimmunoconjugates using Cerenkov luminescence imaging in a disseminated murine leukemia model. Cancer Res 74(20):5846–5854. https://doi.org/10.1158/0008-5472.can-14-0764
30. Altabella L, Boschi F, Spinelli AE (2016) Pixel-based parametric source depth map for Cerenkov luminescence imaging. J Instrum 11:10. https://doi.org/10.1088/1748-0221/11/01/c01048